Published in final edited form as:
Development. 2008 January ; 135(1): 33–41. doi:10.1242/dev.010892.

chongmague reveals an essential role for laminin-mediated boundary formation in chordate convergence and extension movements

Michael T. Veeman[1], **Yuki Nakatani**[1,2], **Carolyn Hendrickson**[1], **Vivian Ericson**[1], **Clarissa Lin**[1], and **William C. Smith**[1,*]

[1] Department of Molecular, Cell and Developmental Biology, University of California Santa Barbara, Santa Barbara CA, 93106, USA

Summary

Although cell intercalation driven by non-canonical Wnt/Planar Cell Polarity (PCP) pathway-dependent mediolateral cell polarity is important for notochord morphogenesis, it is likely that multiple mechanisms shape the notochord as it converges and extends. Here we show that the recessive short-tailed *Ciona savignyi* mutation *chongmague* (*chm*) has a novel defect in the formation of a morphological boundary around the developing notochord. *chm* notochord cells initiate intercalation normally but then fail to maintain their polarized cell morphology and migrate inappropriately to become dispersed in the larval tail. This is unlike *aimless* (*aim*), a mutation in the PCP pathway component Prickle, which has a severe defect in early mediolateral intercalation but forms a robust notochord boundary. Positional cloning identifies *chm* as a mutation in the *C. savignyi* ortholog of the vertebrate alpha 3/4/5 family of laminins. *Cs*-lamα3/4/5 is highly expressed in the developing notochord, and *Cs*-lamα3/4/5 protein is specifically localized to the notochord's outer border. Notochord convergence and extension, reduced but not absent in both *chm* and *aim*, are essentially abolished in the *aim*/*aim; chm*/*chm* double mutant, indicating that laminin-mediated boundary formation and PCP-dependent mediolateral intercalation are each able to drive a remarkable degree of tail morphogenesis in the absence of the other. These mechanisms therefore initially act in parallel, but we also find PCP signaling has an important later role in maintaining the perinotochordal/intranotochordal polarity of *Cs*-lamα3/4/5 localization.

Introduction

Convergence and extension (CE) movements shape chordate embryos such that they become longer along the anteroposterior axis and narrower across the mediolateral axis (Keller, 2002; Wallingford et al., 2002). In vertebrates, CE movements are most pronounced in the tissues that form the notochord, somites and spinal cord. These movements have been best characterized in explanted *Xenopus* dorsal mesoderm, where they include cell intercalation driven by mediolaterally-biased tractive cell protrusions as well as "boundary capture", the tendency of cells to become quiescent on surfaces contacting the nascent notochord/somite boundary (Keller et al., 1989; Shih and Keller, 1992a). Planar cell polarity (PCP) signaling is known to be a key mediator of mediolateral intercalation and related cell behaviors (Veeman et al., 2003; Wang and Nathans, 2007). The molecular basis of morphogenetic behaviors at the notochord boundary are much less well understood, although components of

*Correspondence: w_smith@lifesci.ucsb.edu.
[2]Current Address: Department of Biology, Ochanomizu University, 2-1-1 Otsuka, Bunkyo-ku, Tokyo 112-8610, Japan

the extracellular matrix and integrins have been implicated in directing both motility and boundary behavior (Marsden and DeSimone, 2003; Davidson et al., 2006).

We use the ascidian *Ciona savignyi* as a model for chordate axial morphogenesis, both for the morphological simplicity of its body plan and the genetic simplicity of its compact genome. Ascidian notochord morphogenesis takes place without cell division and involves the intercalation of only 40 notochord cells from an initially isodiametric grouping into a single-file column of flat, disk shaped cells (Cloney, 1964; Miyamoto and Crowther, 1985; Munro et al., 2006; Munro and Odell, 2002b). This intercalation involves mediolaterally-biased tractive cell protrusions, as has also been described in *Xenopus* (Shih and Keller, 1992a; Shih and Keller, 1992b), and may involve a ventrally-oriented invagination movement that helps round the notochord in cross-section (Munro and Odell, 2002b). While this intercalation is essential, a considerable degree of tail extension is also driven by cell shape changes and vacuolization after intercalation is complete (Miyamoto and Crowther, 1985). While notochord intercalation appears broadly similar between ascidians and vertebrates, there are likely important differences between ascidian and vertebrate CE movements. For example, ascidian muscle and neural cells do not obviously play as active and independent a role in CE as they do in vertebrates.

The *Ciona* mutation *aimless* (*aim*) is an allele of the PCP pathway component Prickle (Pk) (Jiang et al., 2005). *aim* notochord cells have severe defects in mediolateral cell polarity and, although fully motile, they converge and extend extremely slowly and incompletely, such that most of the notochord remains roughly two cells wide. The notochord-specific RNA expression (Hotta et al., 2000; Jiang et al., 2005) and mutant phenotype of *aim* suggest that the ascidian PCP pathway is only involved in notochord morphogenesis and not in gastrulation or neural tube closure. Although *aim* is likely a null mutation and has a severe defect in notochord cell behavior, the notochord cells do form a rod-like structure and the tail does show considerable elongation. These observations suggest that multiple mechanisms are important in the overall convergence and extension of the ascidian tail.

A second mutation, *chongmague (chm),* causes a distinct and profound defect in notochord morphogenesis. All 40 notochord cells are present and express notochord-specific genes such as *brachyury* (*bra*), *forkhead* and *tropomyosin* (Deschet et al., 2003; Nakatani et al., 1999), but the notochord cells appear rounded and fail to adopt the wildtype 1×40 “stack of coins” morphology. Markers for other embryonic tissues, including tail muscle, nervous system and epidermis, are correctly expressed within the context of a short and aberrant tail (Deschet et al., 2003; Nakatani et al., 1999). Here we use high-resolution 3D confocal imaging to show that *chm* has a novel and severe defect in the formation of a morphological boundary around the developing notochord. Unlike in *aim*, early intercalation is relatively normal, but the notochord cells lose their polarized morphology and become widely dispersed in the tail.

We hypothesized that the dispersed notochord cells seen in *chm* reflect a failure in boundary capture or some similar behavior at the notochord border. Wildtype ascidian embryos exhibit a suite of complex behaviors at the notochord border, including a surprisingly dynamic boundary capture-like behavior in which notochord cells rapidly spread out on surfaces contacting the boundary. *chm* notochord cells show persistent and undirected motility that is consistent with a failure in this behavior. We have identified *chm* as a mutation in *Cs*-lamα3/4/5, an extracellular matrix (ECM) molecule highly expressed in the notochord and specifically localized to perinotochordal cell surfaces.

Although the notochord boundary can be perturbed by genetic manipulations that transform notochord cells into muscle and vice-versa (Fujiwara et al., 1998; Reintsch et al., 2005), *chm*

is, to the best of our knowledge, the only perturbation with a strong, early and direct effect on the formation of the notochord boundary. *chm* thus provides a unique tool to functionally test the relationship between notochord boundary formation and PCP-dependent cell intercalation. Epistasis analysis suggests that these two mechanisms initially act largely in parallel. The considerable convergence and extension remaining in *aim* is dependent on *chm* function, suggesting that the notochord boundary does not merely support the structural integrity of the notochord and help maintain polarized cell behaviors, but that it can itself drive a significant amount of CE. The relationship between PCP signaling and laminin-mediated boundary formation is not strictly independent, however, as we also observe that the PCP pathway has a role in maintaining the perinotochordal/intranotochordal polarity of *Cs*-lamα3/4/5 localization.

Materials and Methods

Ascidian Culture and Genetics

Mutant ascidian lines were cultured in a running seawater facility as described (Hendrickson et al., 2004). *Ascidiella aspers*a were obtained from the Woods Hole Marine Biological Laboratory. The experiments using the *bra:GFP* transgene used the chm^{35} allele of *chm*, otherwise all experiments used the original *chm* allele.

Antibody and Phalloidin Staining

Embryos were fixed in either 2% paraformaldehyde in sea water or Munro's Ascidian Cytoskeletal Fix (2% paraformaldehyde, 0.1M Hepes pH 7.0, 0.05M EGTA, 0.4M dextrose, 0.01M MgSO4, 0.2% Triton-X), rinsed several times in PBT (PBS+0.2%Triton-X) and fixed in 5% heat-inactivated goat serum in PBT. Bodipy-FL phallacidin (Invitrogen) was used at 1 unit/100μl, anti*Cs*-lamα3/4/5 at 1:250–1:500, rabbit polyclonal anti-GFP at 1:500 and mouse monoclonal anti-GFP at 1:250. The *Cs*-lam α3/4/5 antibody was raised against a bacterially-produced recombinant protein containing amino acids 1330 to 1494 of *Cs*-lamα3/4/5(lam13) fused to an N-terminal His tag. *Cs*-lamα3/4/5 staining required an antigen retrieval step (Kirkpatrick and d'Ardenne, 1984) with 20–40 μg/mL proteinase K in PBT for 4 minutes at 37° followed by several brief washes in PBT on ice. Primary and secondary antibody incubations were overnight at 4°, followed by several washes in PBT. Bodipy-FL phallacidin was used for 1 hour at room temperature in PBT, followed by several washes in PBT. Two color GFP/phalloidin staining used a rabbit polyclonal anti-GFP antibody and a red fluorescent Alexa594 secondary antibody to detect GFP in combination with the green fluorescent Bodipy-FL phallicidin (direct GFP fluorescence is killed by the clearing process). Embryos were cleared and mounted as described (Munro and Odell, 2002b). Electroporations were as described (Corbo et al., 1997).

Imaging

An Olympus Fluoview 500 was used for confocal imaging, using 40x 1.2NA and 60x 1.4NA oil immersion lenses for fixed samples and a 20x 0.7NA air lens for live imaging. Image stacks were at 0.4–0.5 micron spacing for fixed embryos. ImageJ (Wayne Rasband, NIH) was used to reconstruct z sections across the axis of the notochord, and for maximum intensity projections. Slidebook 4.1 (Intelligent Imaging Innovations) was used for volume renderings of confocal stacks. Widefield images were collected using a Leica DMRB compound microscope with a shutter-controlled epifluorescence light path and either a SPOT-2 or a Hamamatsu ERAG CCD camera.

Mapping the *chm* mutation

Bulked segregant analysis (BSA) was performed on DNA isolated from triplicate pools of 15 embryos each from mutant (*chm/chm*) and phenotypically wildtype (wt/wt and wt/*chm*) progeny of a self-fertilized heterozygous *chm* adult, as described previously (Jiang et al., 2005). AFLP reactions on the pooled genomic DNAs were performed using the Small Genome Kit from Invitrogen. The AFLP reactions were resolved on sequencing gels and autoradiographed. Linked bands were eluted from the gels, reamplified, and sequenced using standard fluorescent sequencing methods. Nucleotide sequences of the linked bands were used to search the partially assembled *C. savignyi* genomic sequence.

Cs-lamα3/4/5 Nucleotide Sequence Analysis

Cs-Lamα3/4/5 genomic sequences predicted by paired scaffolds 312 and 44 were used to search protein and nucleic acid databases, including the *C. intestinalis* EST database (Imai et al., 2004). We were able to identify with high confidence N- and C-terminal ESTs for the *C. intestinalis* ortholog of *Cs*-Lamα3/4/5. These *C. intestinalis* EST sequences were then used as guides with the *C. savignyi* genomic sequence to design oligonucleotides to the 5′ and 3′ ends of the *Cs*-Lamα3/4/5 transcript (GAAATATTAGAGTCGCAAAAAACTAGTCAATGACC and GGTCTATGGCGATATTACGACAAATAACTGTCC, respectively). The oligonucleotides were used to amplify an ~11 kbp PCR product using LaTaq (Takara) with cDNA synthesized from RNA extracted from pooled clutches of wildtype *C. savignyi* larvae. Two separate alleles of the wildtype *Cs*-lamα3/4/5 cDNA clones of 11,354 bp (clone *lam13*) and 11,605 bp (clone *lam33*) were sequenced in their entirety, and two conceptual cDNAs were derived from the *C. savignyi* genomic sequence (*haplo1* and *haplo2*). *Cs*-lamα3/4/5 cDNAs from pools of homozygous *chm* and chm^{35} larvae were PCR-amplified in three overlapping fragments. Genomic fragments containing the frameshift mutation identified in the chm^{35} cDNA were PCR-amplified from individual larvae using the oligonucleotides 5′GGAAATGTGCAACCACACG3′ and 5′TCTGTTCTTAAGGTCATTGGCAT3′ and directly sequenced.

Cs-lamα3/4/5 in situ Hybridization

For late-tailbud stage embryos in situ hybridization was as described (Arenas-Mena et al., 2000), using a 986 bp internal cDNA fragment from base 4427 to base 5413 of the lam13 cDNA. For neurula stage embryos a 2032 bp probe from the 3′ end of the fulllength transcript was used as described (Hotta et al., 1999).

Morpholino oligonucleotide knockdown

Fertilized eggs were injected with either sense or anti-sense morpholino oligonucleotides (MO) corresponding to the predicted start codon and flanking 3′-nucleotides of the *Cs*-lamα3/4/5 gene (sense: TCAATGACCAAAATGCTGCGCTTAG; antisense: CTAAGCGCAGCATTTTGGTCATTGA). Eggs were injected with ~15 pL of MO solutions at 0.5 or 0.67 mM (final dose ~10 fmol), as described previously (Imai et al., 2002).

Single tadpole DNA prep

Tadpole larvae were fixed in 3.7% formaldehyde in seawater. After several days in fixative the test cells sloughed off, thus removing any potential maternal DNA contamination. The larvae were then rinsed in distilled water and transferred individually to tubes containing 10 μl of 1% Triton-X 100, 100 mM NaCl, 20 mM Tris pH 7.8, 1 mM EDT, and 1 mg/ml proteinase K. The samples were incubated overnight at 55 °C, followed by a 10 min incubation at 95°C to inactivate the protease.

Results

Early intercalation in *chm* is relatively normal, but the notochord cells fail to maintain polarized cell shapes

Confocal microscopy of a notochord-specific *brachyury:GFP* (*bra:GFP*) transgene (Deschet et al., 2003) in fixed and cleared embryos allows high-resolution analysis of notochord morphogenesis. Although *chm* and *aim* are superficially similar in that both have short tails, the underlying phenotypes are distinct at the cellular level. At early tailbud stage, the earliest stage when *chm* can be identified, considerable convergence and extension have already occurred and the *chm* notochord is only slightly shorter and wider than wildtype (Fig. 1A, B). Identically staged *aim* embryos have undergone little convergence and extension and thus have much shorter, wider notochords (Fig. 1C). *aim* embryos also manifest their mutant phenotype considerably earlier (Jiang et al., 2005; and data not shown). Unlike in wildtype and *aim* embryos, however, the *chm* notochord has an irregular outer border, with many lateral cells elongated along the anteroposterior axis instead of the mediolateral axis (green arrowheads in Fig. 1B).

By mid-tailbud stage, the wildtype notochord has fully intercalated into a compact rod of 40 disc-shaped cells (Fig. 1D, F). In *chm*, however, notochord morphology has become completely aberrant, with rounded, loosely adherent cells forming a dispersed mass in the tail (Fig. 1E, G, H, I). The wildtype notochord is located centrally in the tail, flanked by the dorsal nerve cord, the ventral endodermal strand, and the lateral muscle cells (inset in Fig. 1F). In *chm*, however, notochord cells can be found invading these flanking tissues, most frequently the nerve cord (Fig. 1H) and endodermal strand (Fig. 1I) and occasionally the muscle cells. Supplemental Movies 1 and 2 show rotating 3D renderings of these confocal stacks. *chm* embryos also show a characteristic epidermal protrusion at the tip of the tail (yellow bracket in Fig. 1E, and Supplemental Movie 3).

Ascidian embryos exhibit complex and dynamic behaviors at the notochord boundary

The failure of *chm* notochord cells to either form or respect a morphological boundary between themselves and the flanking tissues is reminiscent of the process of boundary capture that has been described in *Xenopus* embryos, whereby intercalating axial and paraxial mesodermal cells become quiescent on surfaces contacting the nascent notochord/somite boundary (Keller et al., 1989; Shih and Keller, 1992a; Wallingford et al., 2002). Although timelapse studies of ascidian notochord morphogenesis have been reported, none have focused on the morphogenetic processes at the notochord boundary (Miyamoto and Crowther, 1985; Munro and Odell, 2002b). To better characterize these processes in wildtype ascidians, we have made use of the strikingly transparent embryos of *Ascidiella aspersa* (Berrill, 1930), which allow much higher quality DIC imaging than in *Ciona* (Supplemental Movie 4)

At the beginning of intercalation the notochord primordium is difficult to distinguish from the surrounding cells, but as intercalation proceeds it becomes increasingly distinct (Fig. 2A). This is largely a result of the notochord cells each forming a neat, flat edge with the flanking muscle cells. Tracking of individual notochord cells reveals that they do not simply become quiescent on surfaces contacting the boundary, but that they actively and rapidly spread out as they make contact (e.g., the yellow cell as it approaches and contacts the boundary in Fig. 2B). A cell newly contacting the boundary will often partially displace its neighbors before they reestablish an equilibrium of boundary contact (e.g., the green cell displaces its yellow neighbor on contact with the boundary in Fig. 2B). We also note that notochord cell nuclei become polarized away from the notochord boundary (Fig. 2B).

Although this rapid spreading and flattening as notochord cells contact the boundary is suggestive of an adhesive process, the notochord boundary acts as more than simply a substrate for cell adhesion. By tracking the relative positions of notochord and muscle cells over time, it is clear that there is shearing or sliding of cells along this interface (Fig. 2C). Such shearing implies that there must be some active process at work to account for the simultaneous adhesion and movement of cells along the boundary.

We also observe rhythmic pulsatile behaviors at the lateral edges of the notochord cells that persist long after intercalation (Supplemental Movie 4). Miyamoto and Crowther observed a similar behavior in *Ciona*, which they suggested might be a form of blebbing involved in secreting the perinotochordal basement membrane (Miyamoto and Crowther, 1985). In our high-resolution recordings, these pulsatile movements do not appear to be blebbiform in nature, and we hypothesize that they may be involved in breaking and reforming adhesions as the boundary remodels itself during postintercalation tail extension.

chm shows persistent notochord cell motility

Although *Ciona* is not as well suited to live imaging as *Ascidiella*, we were previously able to use timelapse microscopy of the *bra:GFP* transgene to show persistent notochord cell motility in *chm* (Deschet et al., 2003; and Supplemental Movie 5). Those widefield images were unable, however, to resolve individual notochord cells. Here we use confocal microscopy to image GFP-expressing *chm* notochord cells as they migrate to the periphery of the tail (Supplemental Movie 6). In the timelapse sequence shown in Fig. 2D, one small group of cells that is initially contiguous with the main mass of the notochord (blue arrowhead) breaks away and migrates towards the tip of the tail (red arrowhead). These cells show rapid and largely undirected lamelliform protrusions that are absent at this stage in the notochord cells of wildtype siblings (Fig. 2E).

chm is *Cs*-lamα3/4/5

The aberrant cell morphology and movement of the *chm* notochord cells suggests two main hypotheses: *chm* might represent a defect in adhesion between notochord cells or it might reflect a failure to form a basement membrane or other barrier between the notochord and flanking tissues. To distinguish between these and other possibilies, we used Amplified Fragment Length Polymorphism analysis on bulked pools of segregants (AFLP-BSA) to map *chm*, initially finding two potentially linked markers on paired scaffold 44 (now part of reftig 96) and one on paired scaffold 312 (now part of reftig 19) of the partially assembled *C. savignyi* genome (Fig. 3A). An examination of potential open reading frames revealed that these two genomic scaffolds encoded the C- and Nterminal regions, respectively, of a predicted alpha laminin gene. An alpha laminin cDNA that spans these two scaffolds confirmed that they were contiguous. Single strand confirmation polymorphism (SSCP) confirmed tight genetic linkage at the alpha laminin locus (SSCP2; Fig. 3A) and partial linkage near the most distant AFLP marker (SSCP1; Fig. 3A).

Laminins are polymeric heterotrimers of large alpha, beta and gamma chains that are important components of the basement membranes (basal laminae) that serve to adhere cells and separate tissues (Sasaki et al., 2004). Given that *chm* is defective in forming a morphological boundary between the notochord and its flanking tissues, a basement membrane component such as a laminin was a strong candidate gene. A phylogenetic analysis revealed that this gene was one of only two *C. savignyi* alpha laminins, and was most closely related to vertebrate alpha 3, 4, and 5 laminins (Supplemental Fig. 1). Accordingly, we have named it *Cs*-lamα3/4/5.

In situ hybridization against *Cs*-lamα3/4/5 message shows that it is strongly expressed in the notochord during tail extension (Fig. 3B,C,D). There is also faint expression throughout the tail and the epidermis at later stages. In *chm*, *Cs*-lamα3/4/5 RNA expression is greatly reduced and the strong notochord-specific expression is eliminated (Fig. 3F). Both the strong notochordal expression and the decreased expression in *chm* mutant embryos are consistent with *Cs*-lamα3/4/5 being *chm*.

To further investigate *Cs*-lamα3/4/5 as a candidate for *chm*, fertilized eggs were injected with either sense or antisense morpholino oligonucleotides (MO) corresponding to the predicted start codon and adjacent 3′-nucleotides of *Cs*-lamα3/4/5. The majority of embryos injected with the antisense MO showed a short tail and epidermal protrusion phenotype characteristic of *chm* [74% (n=23) and 83% (n=24), for two independent experiments]. The two larvae presented in Fig. 3H and I show the range of phenotypes observed, which closely mirrors the range of phenotypes seen in *chm*/*chm* embryos. In contrast, none of the embryos injected with the control sense MO showed this *chm*-like phenotype (n= 62 and 99, for the two experiments, and Fig. 3G). To further examine the morphant phenotype, we also injected the *Cs*-lamα3/4/5 antisense morpholino into eggs fertilized with sperm carrying the *bra:GFP* transgene. This revealed an irregular notochord boundary with notochord cells widely dispersed in the tail (Fig. 3J), exactly as seen in the *chm* mutant (Fig. 1E). Other aspects of *chm* are also closely phenocopied, including the formation of a long epidermal protrusion at the tip of the tail.

Sequencing of *Cs*-lamα3/4/5 cDNAs from *chm* and two wildtype alleles revealed multiple nonsynonymous polymorphisms, and a splicing variation found only in *chm* that creates a 9 amino acid insertion (Fig. 3K). A second non-complementing allele, chm^{35}, was isolated in a screen for spontaneous mutations in the wild *C. savignyi* population (Hendrickson et al., 2004). chm^{35} is phenotypically indistinguishable from *chm*, and also shows tight genetic linkage to Cs-lamα3/4/5 (Supplemental Fig. 2). Nucleotide sequence analysis of *Cs*-lamα3/4/5 cDNA and genomic DNA from chm^{35} identified a frameshift mutation early in the laminin I domain predicted to cause truncation of nearly half the protein (Fig. 3K,L). The tight genetic linkage, expression pattern, reduced expression in *chm*, morpholino phenocopy, and definitive frameshift mutation in chm^{35} all support the conclusion that the two alleles of *chm* both have lesions in the *Cs*-lamα3/4/5 gene.

Cs-lamα3/4/5 protein is localized to perinotochordal surfaces

Given the *chm* phenotype, we hypothesized that *Cs*-lamα3/4/5 might be a component of a perinotochordal extracellular matrix (ECM). Perinotochordal basement membranes have been described in the mature notochords of many species, where they are thought to form an inelastic sheath that opposes the turgor pressure generated by vacuolization (Stemple, 2005). Earlier developmental roles for perinotochordal ECM molecules are not as well established. Perinotochordal ECM has been observed in *Ciona* embryos by electron microscopy as early as tailbud stage, but does not form a thick, multilayered basement membrane until much later, during vacuolization (Cloney, 1964). Although the molecular composition of the ascidian perinotochordal ECM is unknown, laminins are known to be important components of the zebrafish perinotochordal basement membrane (Scott and Stemple, 2005).

We raised a rabbit polyclonal antibody against a bacterially expressed segment of *Cs*-lamα3/4/5 that is not conserved in the second *C. savignyi* alpha laminin gene. Staining is first evident at neurula stage as a faint, irregular outline around the outside of the notochord primordium (Fig. 4A). By early tailbud stage there is robust staining around the notochord primordium as well as expression between the epidermis and the underlying tissues (Fig. 4B). By late tail extension stage the perinotochordal staining is stronger yet (Fig. 4C). In tangential optical sections, longitudinal fibers can be seen along the notochord surface (Fig.

4D). In reconstructed z-sections, the strongest staining is around the notochord, but it is also demarcates all of the major tissues in the tail: notochord, muscle, epidermis, nerve cord and endodermal strand (Fig 4E). There is also peripheral epidermal staining that is somewhat variable dependent on the proteinase treatment necessary to unmask the laminin epitope.

In *chm* embryos, staining is still evident but noticeably decreased. The perinotochordal staining in particular is weak and patchy (Fig. 4F). As further controls for antibody specificity, preblocking the antibody with recombinant antigen greatly decreases the observed staining, and little to no staining is seen in embryos stained with non-immune rabbit serum (Fig. 4K). Mosaic overexpression of full-length *Cs*-lamα3/4/5 by electroporation also gives rise to increased staining in the expressing cells (Fig. 4L,M). We conclude that the antibody is a faithful probe for *Cs*-lamα3/4/5 protein localization and that the perinotochordal staining observed is fully consistent with a role as a perinotochordal basement membrane component involved in notochord boundary formation. The subectodermal staining is also consistent with the epidermal tail protrusion phenotype, which likely involves decreased adhesion between the ectoderm and underlying tissues.

Cs-lamα3/4/5 polarity is perturbed in the PCP mutant *aim*

To examine potential interactions between the planar cell polarity pathway and laminin-mediated boundary formation, we stained *aim* embryos with the *Cs*-lamα3/4/5 antibody. The perinotochordal staining remained robust but we also observed large patches of staining deep within the notochord, between adjacent cells (Fig. 4G–J). This internal laminin expression was typically quite mild at early stages and became progressively more severe over time, suggesting that PCP signaling is involved in maintenance rather than establishment of *Cs*-lamα3/4/5 polarization.

Laminin-mediated boundary formation can drive considerable tail elongation in the absence of PCP signaling

The observation of ectopic intranotochordal laminin in *aim* embryos caused us to reconsider aspects of the *aim* phenotype. It was previously shown that *aim* notochord cells have a near-complete loss of the mediolateral bias in actin-rich cell protrusions thought to drive intercalation (Jiang et al., 2005; Munro and Odell, 2002b). Such measurements were only made, however, very early in the process of intercalation, and the *aim* notochord does continue to intercalate, albeit very slowly, such that it eventually becomes approximately two cells wide.

In Fig. 5A and B, we compare an early tailbud stage wildtype embryo with a considerably (~2hrs) older *aim* embryo, so as to compare embryos at a similar degree of intercalation. (A wildtype embryo of identical age to Fig. 5B has already completed intercalation, as shown in Fig. 1D,F.). Although they have notochords of roughly comparable length and width, the *aim* notochord cells are less mediolaterally elongated than in wildtype, and they fail to polarize their nuclei away from the notochord boundary. Despite these differences, the *aim* notochord cells are, in many respects, relatively normal: they form a neat, flat edge with the flanking muscle cells; they show a degree of mediolateral elongation; and they typically show concentrations of actin on medial cell surfaces opposite the notochord boundary and not on their anterior and posterior edges (white arrowheads in Fig. 5B).

We hypothesized that the considerable degree of notochord morphogenesis in *aim* might be the result of *Cs*-lamα3/4/5-mediated boundary formation, given that *aim* embryos form a smooth and compact notochord boundary. To test this hypothesis, we constructed the *aim*/*aim;chm*/*chm* double mutant. Unlike either single mutant, the double mutant shows essentially no tail extension (Fig. 5C), but still has the normal number of *brachyury*-

expressing notochord cells (Fig. 5D and data not shown; see Supplemental Fig. 3 for molecular genotyping of these phenotypic classes). With the exception of a small number of notochord cells that migrate between the two blocks of muscle cells (likely the secondary notochord lineage), the majority of notochord cells remain in an isodiametric group comparable to the wildtype notochord primordium prior to the onset of intercalation (compare Fig. 5D and 5E). Having shown that laminin-mediated boundary formation is sufficient to drive considerable tail elongation in the absence of PCP signaling, one question that remains is why *aim* embryos fail to complete intercalation, given that they do slowly develop polarized cell morphologies. We would suggest that this may reflect the observed failure to maintain the perinotochordal/intranotochordal polarity of ECM proteins such as laminin, giving rise to an ectopic basement membrane on intranotochordal surfaces and preventing further intercalation. See Fig. 6 for a diagram of this model.

Discussion

Importance of the Perinotochordal Boundary

Although not well understood on a cellular or molecular level, there is considerable evidence that the notochord boundary is of great importance in shaping the converging and extending mesoderm. Keller and colleagues initially described how intercalating *Xenopus* mesoderm cells are “captured” such that they become quiescent on cell surfaces contacting the notochord/somite boundary (Keller et al., 1989; Shih and Keller, 1992a). In ascidian embryos, Munro and Odell used explant and ablation studies to demonstrate that the notochord primordium requires certain contacts with neighboring tissues in order to converge and extend (Munro and Odell, 2002a). Ascidian tail extension can also be perturbed by misexpression of a Snail-VP16 construct that gives rise to notochord fate in a subset of muscle cells, suggesting that the orderly physical arrangement of the notochord/muscle boundary is essential (Fujiwara et al., 1998). Here we have shown that the ascidian notochord boundary supports several complex behaviors: a dynamic spreading behavior as notochord cell surfaces are captured by the boundary; shearing along the boundary between the notochord and muscle cells; rhythmic pulsatile movements after intercalation is complete; and, most significantly, considerable convergence and extension of the notochord, even in the absence of a functional PCP pathway.

While numerous genetic, pharmacological and embryological approaches have been used to study notochord development in many model systems, the severe phenotype seen in *chm* has not been described in other contexts. In *Xenopus* embryos, perturbations of perinotochordal ECM molecules such as fibrillin and fibronectin cause convergent extension phenotypes that may reflect defects in boundary capture, but do not cause a wholesale disruption of the notochord boundary as seen in *chm* (Davidson et al., 2006; Skoglund and Keller, 2006). We would suggest that laminins be considered as candidate vertebrate boundary capture signals.

The three-dimensional tissue architecture of the converging and extending ascidian notochord is quite complex. As it narrows and lengthens, it not only intercalates but also undergoes a ventrally-oriented invagination movement that transforms it from a sheet to a rod (Munro and Odell, 2002b). Although it is clear that morphogenetic processes at the notochord boundary are of great importance in shaping the ascidian notochord, it is not clear if there is a morphologically distinct population of border cells. It is possible that all notochord cells are, at some dorsoventral position, in partial contact with the nascent perinotochordal boundary from the earliest stages, and that what is presented in Fig. 6 as cells being trapped *de novo* by the boundary actually represents cells expanding the fraction of their periphery in contact with the boundary. Competition for an initially limiting expanse of bounding surfaces may help explain the extreme length-to-width ratios (Munro and Odell, 2002b) of the disc-shaped cells in the justintercalated notochord.

Laminins in notochord morphogenesis

Although it is possible that a specific role for laminin in notochord boundary formation is unique to the ascidians, we would argue that the novelty of the *chm* phenotype likely reflects the morphological simplicity of the ascidian embryo and the genomic simplicity of its complement of ECM components. In vertebrates, for example, there are typically 5 alpha, 4 beta and 3 gamma laminin subunits (Li et al., 2003), as opposed to 2 alpha, 1 beta and 1 gamma in ascidians (Sasakura et al., 2003). Analysis of the large set of murine laminins has been complicated by essential early roles in preimplantation development in addition to considerable redundancy and compensation between various family members (Li et al., 2003). Laminins are clearly important for vertebrate notochord development as indicated by the zebrafish mutations *bashful* (lamα1), *grumpy* (lamβ1) and *sleepy* (lamγ1), which have later roles in notochord differentiation (Parsons et al., 2002; Pollard et al., 2006). While *grumpy* and *sleepy* mutants show a nearly complete absence of reactivity to a mouse laminin-1 antibody (Parsons et al., 2002), it is likely that there is still considerable functional redundancy between the zebrafish laminins that may mask a more *chm*-like phenotype. For example, injection of lamα5 morpholino into *bashful* causes a severe disruption of notochord and other tissues that has not been characterized in detail (Pollard et al., 2006). A convergent extension phenotype has also been seen in zebrafish embryos depleted of a galactosyltransferase important in posttranslational modifications of laminin (Machingo et al., 2006).

PCP signaling and the ECM

Recent work suggests that there may be important interactions between vertebrate PCP signaling and the extracellular matrix. The PCP proteins Prickle, Strabismus and Dishevelled have been shown to be important in restricting fibronectin protein localization to the outer surfaces of the *Xenopus* notochord (Goto et al., 2005), similar to what we observe with laminin localization in the *Cs*-pk mutation *aim*. Tissue separation defects have also been described in *Xenopus* and zebrafish embryos with perturbed non-canonical Wnt/PCP signaling (Ulrich et al., 2003; Winklbauer et al., 2001). It may be of considerable interest to look for defects in polarized ECM deposition in zebrafish PCP mutants and other contexts that have previously been interpreted strictly in terms of perturbed cell motility.

Interactions between PCP signaling and laminin-mediated boundary formation

Unlike in *aim* mutants, early notochord intercalation in *chm* is relatively normal and then becomes progressively more aberrant, suggesting that one role of the notochord boundary is to maintain polarized cell behaviors initiated by PCP signaling. *Cs*-lam α3/4/5-mediated boundary formation is able, however, to cause considerable narrowing and lengthening of the notochord even in the absence of a functional PCP pathway, as indicated by the near-complete loss of convergence and extension in the *aim*/*aim;chm*/*chm* double mutant as compared to *aim*/*aim*. As prickle and and *Cs*-lam α3/4/5 are predominantly expressed in the notochord, the severity of this phenotype suggests that the ascidian muscle and neural plate do not have a strong ability to autonomously converge and extend as seen in vertebrates.

Although the double mutant phenotype indicates that *aim* and *chm* act largely in parallel, the observation of intranotochordal laminin in *aim* embryos suggests that there is a more complex relationship. As this intranotochordal staining is initially minimal and becomes progressively stronger over time, it appears that PCP signaling is involved in the maintenance rather than the initial establishment of perinotochordal ECM polarity. The *aim* mutation truncates much of the *Cs*-Pk protein, causes a complete loss of membrane localization of the PCP effector molecule Dishevelled, and shows no maternal effect (Jiang et al., 2005), so the *aim* phenotype likely reflects a complete loss of Pk function. We cannot fully exclude, however, that there may be residual function in *chm* or *aim* that might

confound epistatis analysis. It will be of great interest to determine whether perinochordal laminin localization involves polarized secretion, stabilization or degradation, and how later perinotochordal/intranotochordal polarity relates to earlier mediolateral polarity. We would suggest that PCP signaling has multiple distinct functions in ascidian notochord morphogenesis, including an early role in the mediolateral polarity of tractive cell protrusions (Jiang et al., 2005), a subsequent role in maintaining polarized ECM localization (this study), a role in polarizing cell nuclei away from the boundary late in intercalation (this study), and a role in anteroposterior polarity after intercalation is complete (Jiang et al., 2005). Advanced imaging methods will likely be of great importance in supporting and extending these models of notochord morphogenesis.

Supplementary Material

Refer to Web version on PubMed Central for supplementary material.

Acknowledgments

We thank Matt Kourakis and Wendy Reeves for helpful comments on the manuscript and William Graham and Hank Hymanson for their assistance in identifying carriers. This work was supported by NIH grants HD038701 and GM075049 to WCS and a Santa Barbara Foundation/Tri-County Blood Bank Fellowship to MTV.

References

Arenas-Mena C, Cameron AR, Davidson EH. Spatial expression of Hox cluster genes in the ontogeny of a sea urchin. Development 2000;127:4631–43. [PubMed: 11023866]

Berrill NJ. Studies in Tunicate Development. Part I. General Physiology of Development of Simple Ascidians. Philosophical Transactions of the Royal Society of London. Series B, Containing Papers of a Biological Character 1930;218:37–78.

Cloney RA. Development of the ascidian notochord. Acta Embryologie et Morphologie Experimentalis 1964;7:111–130.

Corbo JC, Levine M, Zeller RW. Characterization of a notochord-specific enhancer from the Brachyury promoter region of the ascidian, *Ciona intestinalis*. Development 1997;124:589–602. [PubMed: 9043074]

Davidson LA, Marsden M, Keller R, Desimone DW. Integrin alpha5beta1 and fibronectin regulate polarized cell protrusions required for *Xenopus* convergence and extension. Curr Biol 2006;16:833–44. [PubMed: 16682346]

Deschet K, Nakatani Y, Smith WC. Generation of Ci-Brachyury-GFP stable transgenic lines in the ascidian *Ciona savignyi*. Genesis 2003;35:248–59. [PubMed: 12717736]

Foernzler D, Beier DR. Gene mapping in zebrafish using single-strand conformation polymorphism analysis. Methods Cell Biol 1999;60:185–93. [PubMed: 9891338]

Fujiwara S, Corbo JC, Levine M. The snail repressor establishes a muscle/notochord boundary in the *Ciona* embryo. Development 1998;125:2511–20. [PubMed: 9609834]

Goto T, Davidson L, Asashima M, Keller R. Planar cell polarity genes regulate polarized extracellular matrix deposition during frog gastrulation. Curr Biol 2005;15:787–93. [PubMed: 15854914]

Hendrickson C, Christiaen L, Deschet K, Jiang D, Joly JS, Legendre L, Nakatani Y, Tresser J, Smith WC. Culture of adult ascidians and ascidian genetics. Methods Cell Biol 2004;74:143–70. [PubMed: 15575606]

Hotta K, Takahashi H, Asakura T, Saitoh B, Takatori N, Satou Y, Satoh N. Characterization of Brachyury-downstream notochord genes in the *Ciona intestinalis* embryo. Dev Biol 2000;224:69–80. [PubMed: 10898962]

Hotta K, Takahashi H, Erives A, Levine M, Satoh N. Temporal expression patterns of 39 Brachyury-downstream genes associated with notochord formation in the *Ciona intestinalis* embryo. Dev Growth Differ 1999;41:657–64. [PubMed: 10646795]

Imai KS, Hino K, Yagi K, Satoh N, Satou Y. Gene expression profiles of transcription factors and signaling molecules in the ascidian embryo: towards a comprehensive understanding of gene networks. Development 2004;131:4047–58. [PubMed: 15269171]

Imai KS, Satou Y, Satoh N. Multiple functions of a Zic-like gene in the differentiation of notochord, central nervous system and muscle in *Ciona savignyi* embryos. Development 2002;129:2723–32. [PubMed: 12015299]

Jiang D, Munro EM, Smith WC. Ascidian prickle regulates both mediolateral and anterior-posterior cell polarity of notochord cells. Curr Biol 2005;15:79–85. [PubMed: 15700379]

Keller R. Shaping the vertebrate body plan by polarized embryonic cell movements. Science 2002;298:1950–4. [PubMed: 12471247]

Keller R, Cooper MS, Danilchik M, Tibbetts P, Wilson PA. Cell intercalation during notochord development in *Xenopus laevis*. J Exp Zool 1989;251:134–54. [PubMed: 2769201]

Kirkpatrick P, d'Ardenne AJ. Effects of fixation and enzymatic digestion on the immunohistochemical demonstration of laminin and fibronectin in paraffin embedded tissue. J Clin Pathol 1984;37:639–44. [PubMed: 6427296]

Li S, Edgar D, Fassler R, Wadsworth W, Yurchenco PD. The role of laminin in embryonic cell polarization and tissue organization. Dev Cell 2003;4:613–24. [PubMed: 12737798]

Machingo QJ, Fritz A, Shur BD. A beta1,4-galactosyltransferase is required for convergent extension movements in zebrafish. Dev Biol 2006;297:471–82. [PubMed: 16904099]

Marsden M, DeSimone DW. Integrin-ECM interactions regulate cadherin-dependent cell adhesion and are required for convergent extension in *Xenopus*. Curr Biol 2006;13:1182–1191. [PubMed: 12867028]

Miyamoto DM, Crowther RJ. Formation of the notochord in living ascidian embryos. J Embryol Exp Morphol 1985;86:1–17. [PubMed: 4031734]

Munro E, Robin F, Lemaire P. Cellular morphogenesis in ascidians: how to shape a simple tadpole. Curr Opin Genet Dev 2006;16:399–405. [PubMed: 16782323]

Munro EM, Odell G. Morphogenetic pattern formation during ascidian notochord formation is regulative and highly robust. Development 2002a;129:1–12. [PubMed: 11782396]

Munro EM, Odell GM. Polarized basolateral cell motility underlies invagination and convergent extension of the ascidian notochord. Development 2002b;129:13–24. [PubMed: 11782397]

Nakatani Y, Moody R, Smith WC. Mutations affecting tail and notochord development in the ascidian *Ciona savignyi*. Development 1999;126:3293–301. [PubMed: 10393109]

Parsons MJ, Pollard SM, Saude L, Feldman B, Coutinho P, Hirst EM, Stemple DL. Zebrafish mutants identify an essential role for laminins in notochord formation. Development 2002;129:3137–46. [PubMed: 12070089]

Pollard SM, Parsons MJ, Kamei M, Kettleborough RN, Thomas KA, Pham VN, Bae MK, Scott A, Weinstein BM, Stemple DL. Essential and overlapping roles for laminin alpha chains in notochord and blood vessel formation. Dev Biol 2006;289:64–76. [PubMed: 16321372]

Reintsch WE, Habring-Mueller A, Wang RW, Schohl A, Fagotto F. Beta-catenin controls cell sorting at the notochord-somite boundary independently of cadherin-mediated adhesion. J Cell Biol 2005;170:675–86. [PubMed: 16103232]

Saitou N, Nei M. The neighbor-joining method: a new method for reconstructing phylogenetic trees. Mol Biol Evol 1987;4:406–25. [PubMed: 3447015]

Sasaki T, Fassler R, Hohenester E. Laminin: the crux of basement membrane assembly. J Cell Biol 2004;164:959–63. [PubMed: 15037599]

Sasakura Y, Shoguchi E, Takatori N, Wada S, Meinertzhagen IA, Satou Y, Satoh N. A genomewide survey of developmentally relevant genes in *Ciona intestinalis*. X. Genes for cell junctions and extracellular matrix. Dev Genes Evol 2003;213:303–13. [PubMed: 12740697]

Scott A, Stemple DL. Zebrafish notochordal basement membrane: signaling and structure. Curr Top Dev Biol 2005;65:229–53. [PubMed: 15642386]

Shih J, Keller R. Cell motility driving mediolateral intercalation in explants of *Xenopus laevis*. Development 1992a;116:901–14. [PubMed: 1295743]

Shih J, Keller R. Patterns of cell motility in the organizer and dorsal mesoderm of Xenopus laevis. Development 1992b;116:915–30. [PubMed: 1295744]

Skoglund P, Keller R. *Xenopus* fibrillin regulates directed convergence and extension. Dev Biol. 2006

Stemple DL. Structure and function of the notochord: an essential organ for chordate development. Development 2005;132:2503–12. [PubMed: 15890825]

Ulrich F, Concha ML, Heid PJ, Voss E, Witzel S, Roehl H, Tada M, Wilson SW, Adams RJ, Soll DR, et al. Slb/Wnt11 controls hypoblast cell migration and morphogenesis at the onset of zebrafish gastrulation. Development 2003;130:5375–84. [PubMed: 13129848]

Veeman MT, Axelrod JD, Moon RT. A second canon. Functions and mechanisms of beta-catenin-independent Wnt signaling. Dev Cell 2003;5:367–77. [PubMed: 12967557]

Wallingford JB, Fraser SE, Harland RM. Convergent extension: the molecular control of polarized cell movement during embryonic development. Dev Cell 2002;2:695–706. [PubMed: 12062082]

Wang Y, Nathans J. Tissue/planar cell polarity in vertebrates: new insights and new questions. Development 2007;134:647–58. [PubMed: 17259302]

Winklbauer R, Medina A, Swain RK, Steinbeisser H. Frizzled-7 signalling controls tissue separation during *Xenopus* gastrulation. Nature 2001;413:856–60. [PubMed: 11677610]

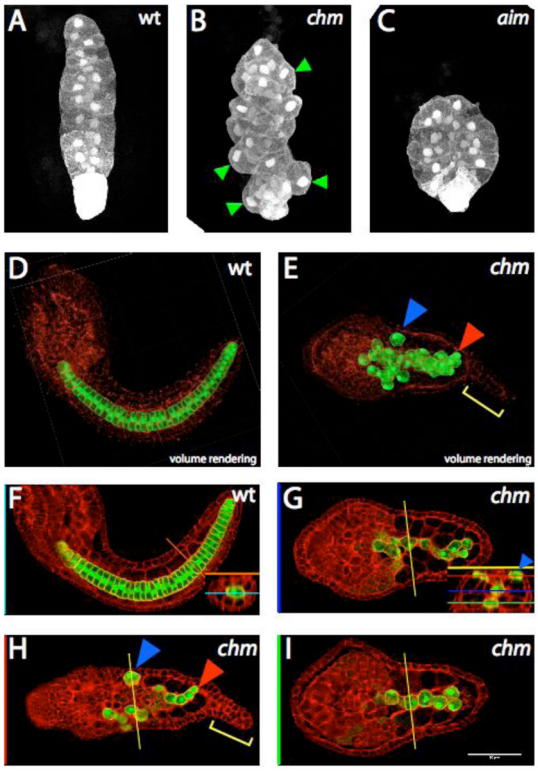

Fig. 1. Notochord morphology in *chongmague*

All images show the notochord-specific *bra:GFP* transgene (white in A–C, green in D–I). Although not fused to any localization signal, the GFP is consistently brighter in the nucleus and cell cortex, and also brighter in the eight secondary lineage notochord cells at the posterior tip of the tail. Panels D–I also show the actin cytoskeleton labeled with phallacidin in red.

(A–C) Maximum intensity projections of confocal stacks through identically staged wildtype (A), *chm*/*chm* (B), and *aim*/*aim* (C) embryos. Anterior to the top. Green arrowheads in B show notochord cells at the edges of the notochord that have their long axes inappropriately oriented along the anteroposterior and not the mediolateral axis. (D, F) Mid-tailbud stage wildtype embryo. Anterior is to the left. (D) is a volume rendering of the entire confocal stack and (F) is a single slice at the level indicated by the blue line (inset). The inset shows a cross section along the orange line in the main panel. (E,G–I) *chm*/*chm* sibling. Anterior is to the left. (E) is a volume rendering and (G–I) are single slices at the levels indicated on the cross-section inset in G. The blue arrowheads mark an isolated notochord cell at the periphery of the tail. The red arrowhead marks a notochord cell interdigitated between two muscle cells. The yellow bracket marks the characteristic epidermal protrusion at the tip of the *chm* tail.

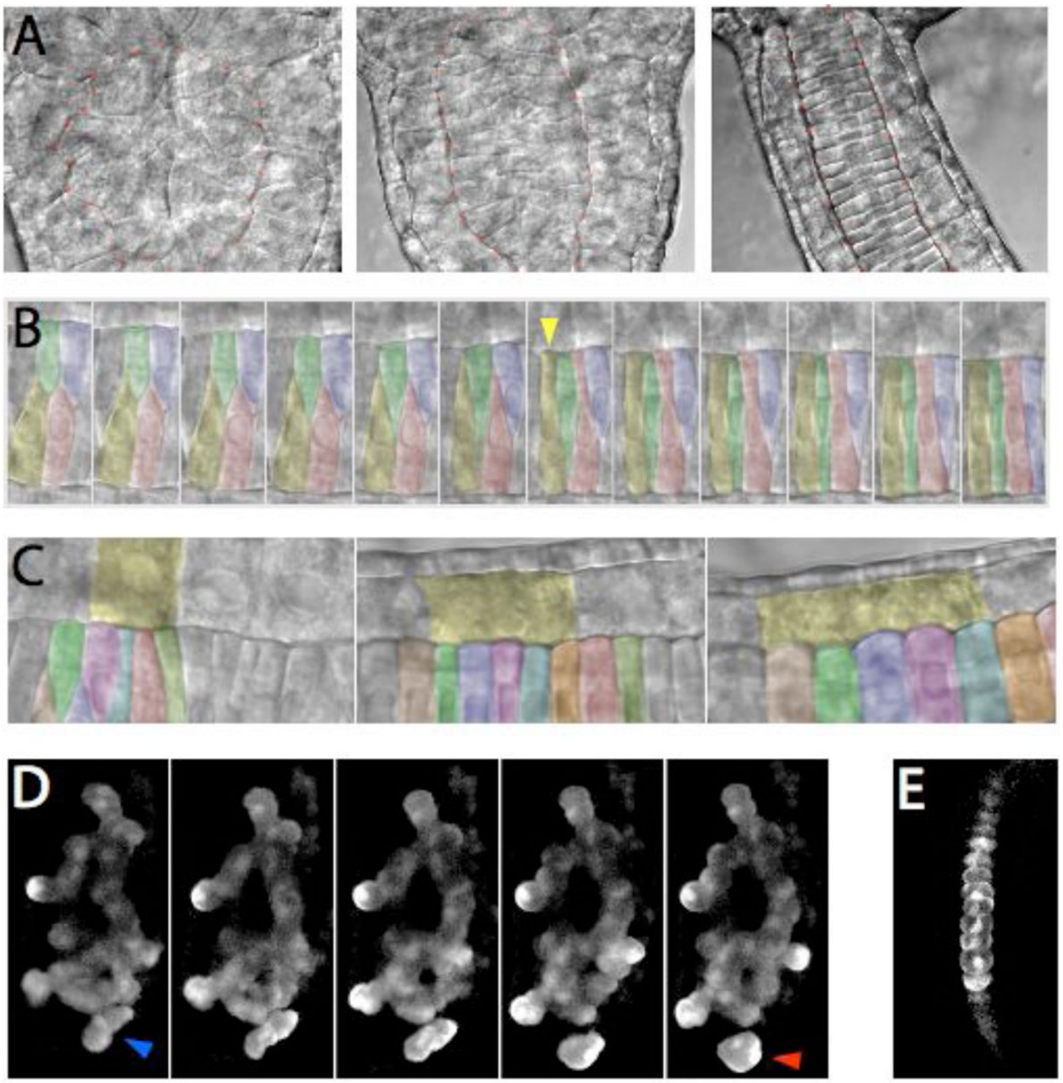

Fig. 2. Timelapse analysis of ascidian notochord boundary formation

(A–C) Nomarski timelapses of notochord boundary formation in the highly transparent ascidian *Ascidiella aspersa*.

(A) Emergence of a morphologically distinct notochord boundary (marked with orange dots). Frames are 100 minutes apart.

(B) Cell behaviors at the notochord boundary late in intercalation. Note the rapid spreading of the yellow cell as it contacts the boundary (indicated by the yellow arrowhead), while the adjacent green cell becomes temporarily displaced. Frames are 3 minutes apart.

(C) Gradual shearing of muscle cells (one marked in yellow) versus notochord cells along the notochord boundary. Frames are 75 minutes apart.

(D) Confocal timelapse of *bra:GFP* fluorescence in a *chm*/*chm Ciona savignyi* embryo. Anterior is to the top. Note the small group of cells in the first frame (blue arrow) that break away from the main mass of the notochord and migrate towards the tip of the tail (red arrow in the final frame). There is also considerable movement of cells at the notochord boundary, especially on the bottom right side of the image. Frames shown are 16 min apart.

(E) shows a single frame of *bra:GFP* fluorescence in a wildtype sibling imaged just after the timelapse in D was completed.

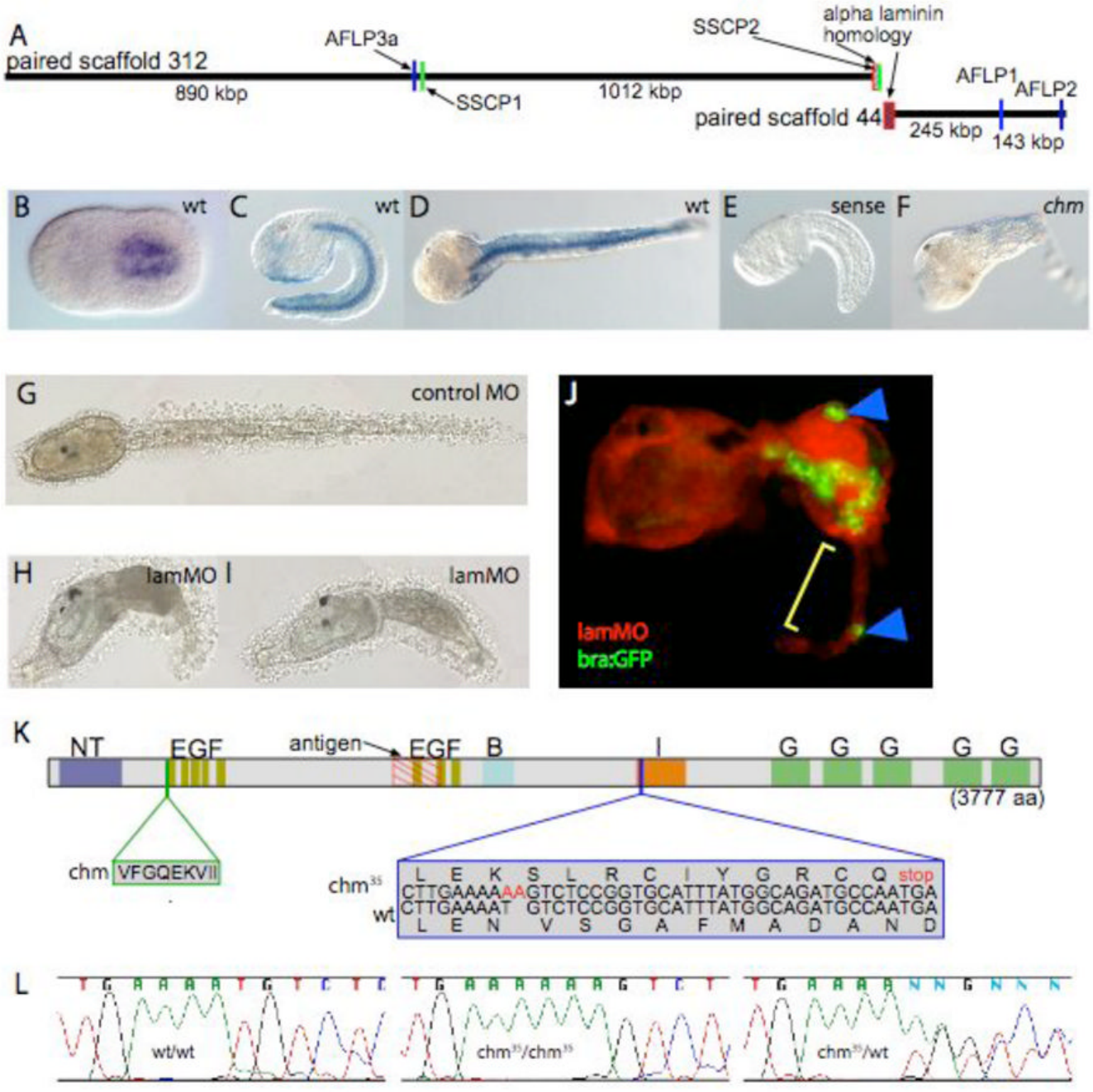

Fig. 3. *Chm* is *Cs*-lamα3/4/5

(A) Schematic of AFLP and SSCP mapping showing a predicted alpha laminin gene on paired scaffolds 312 and 44.

(B–D) Wholemount in-situ hybridization for *Cs*-lamα3/4/5 message showing notochord-specific expression in (B) late neurula, (C) mid-tailbud and (D) late tail extension stages.

(E) shows a sense control and (F) shows decreased expression in a *chm*/*chm* embryo.

(G) Embryo injected with control morpholino

(H,I) *Cs*-lamα3/4/5 morphant embryos showing the range of phenotypes observed.

(J) *bra:GFP* expressing embryo coinjected with *Cs*-lamα3/4/5 morpholino and red fluorescent dextran as an injection marker. Note the disorganized notochord boundary, the

dispersed bra:GFP expressing cells in the tail (blue arrowheads) and the characteristic epidermal protrusion (yellow bracket).

(K) Schematic of *Cs*-lamα3/4/5 domain structure showing a 9 amino acid insertion in *chm* and a frameshift predicted to cause to premature termination in chm^{35}. The antigen used to make the *Cs*-lamα3/4/5 antibody is indicated.

(L) Chromatograms showing the chm^{35} frameshift in genomic DNA from wt/wt, chm^{35}/chm^{35} and chm^{35}/wt individuals.

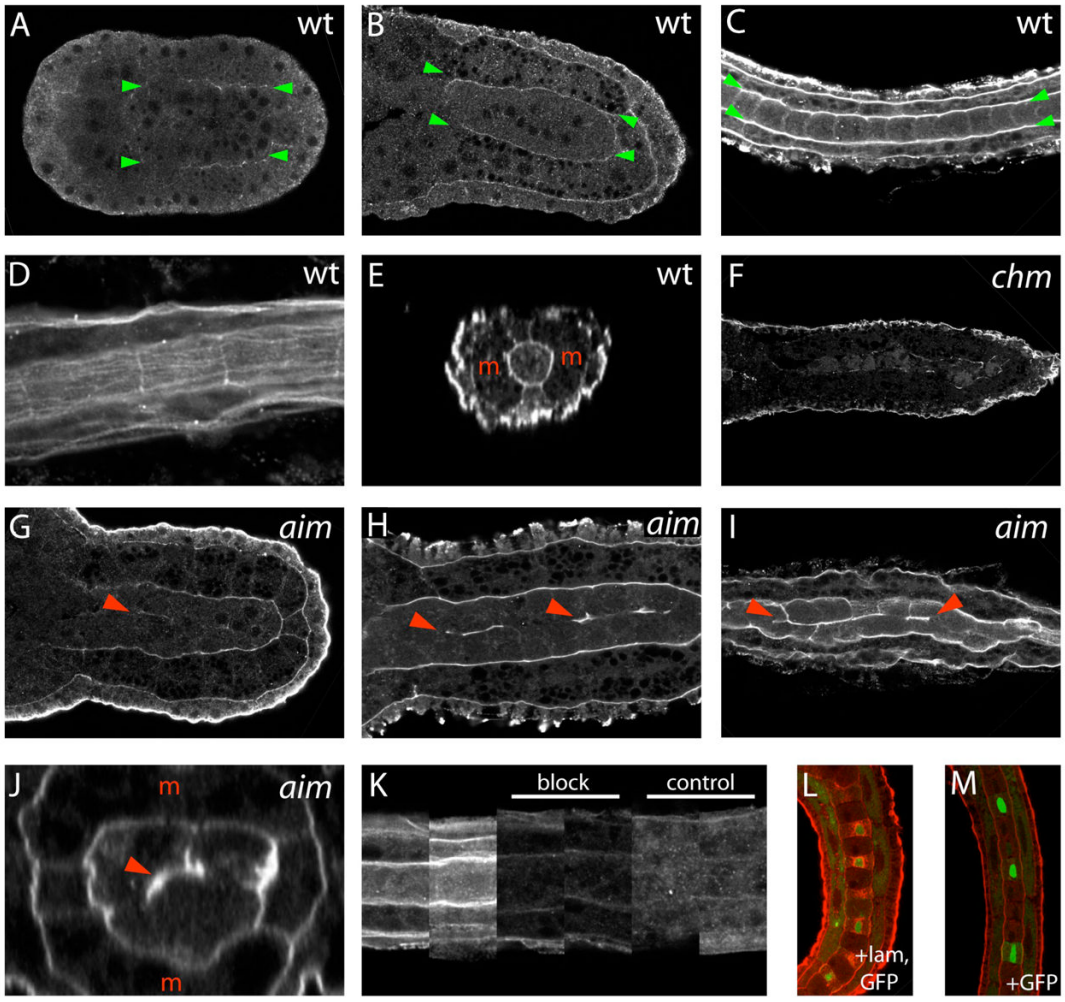

Fig. 4. Immunolocalization of *Cs*-lamα3/4/5

(A–C) Single confocal sections through the notochords of wildtype embryos stained for *Cs*-lamα3/4/5 at (A) late neurula, (B) early tailbud, and (C) late tail stages. Anterior is to the left. Green arrowheads indicate the lateral edges of the notochord or notochord primordium.

(D) Tangential section grazing the perinotochordal surface of a wildtype late tail stage embryo.

(E) Reconstructed Z section across the notochord of a mid-tail wildtype embryo. Red ‘m’s indicate the lateral blocks of muscle cells.

(F) Single confocal section through the notochord of a mid-tail stage *chm*/*chm* embryo.

(G–I) Single confocal sections through the notochords of (G) mid-tail, (H) mid-late tail and (I) late tail stage *aim*/*aim* embryos. Red arrowheads show ectopic laminin localization on intranotochordal cell surfaces.

(J) Reconstructed Z section across the notochord of an *aim*/*aim* mid-late tail stage embryo. Red ‘m’s indicate the lateral blocks of muscle cells, and the red arrowhead shows ectopic laminin.

(K) shows representative images from multiple wildtype embryos stained under standard conditions with the *Cs*-lamα3/4/5 antibody, the *Cs*-lamα3/4/5 antibody blocked by prebinding to *Cs*-lamα3/4/5 peptide, or with control non-immune normal rabbit serum.

(L,M) *Cs*-lamα3/4/5 antibody staining (red) and GFP staining (green) in *C. intestinalis* embryos electroporated with (L) notochord-specific expression plasmids for both *Cs*-lam α3/4/5 and GFP, or (M) GFP plasmid alone.

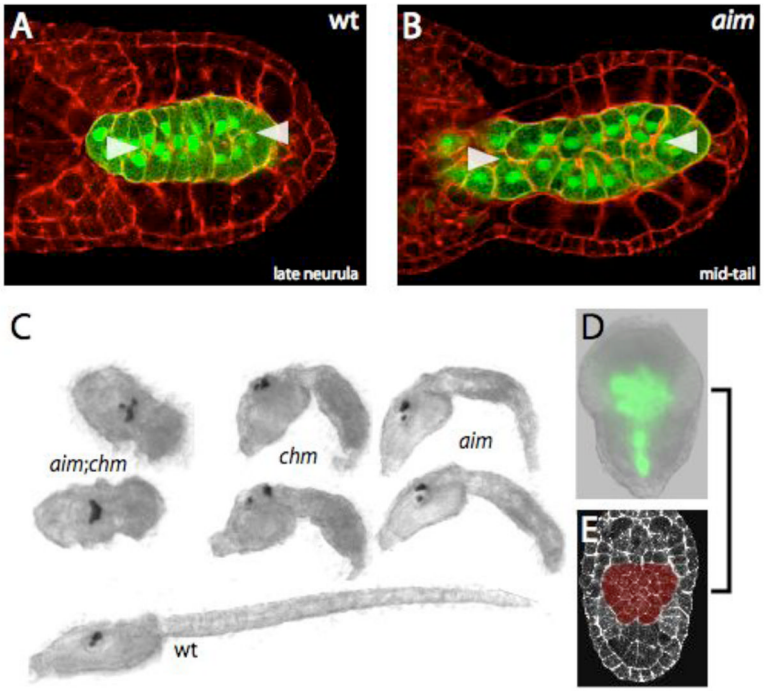

Fig. 5. *Cs*-lamα3/4/5 can drive considerable tail extension in the absence of a functional PCP pathway

(A,B) Confocal section through (A) late neurula stage wildtype embryo and (B) mid-tail stage *aim*/*aim* embryo. Anterior to the left. *bra:GFP* in green, phallacidin in red. White arrowheads indicate medially polarized actin-rich structures.

(C) Brightfield images of hatched larvae of the indicated genotypes.

(D) Widefield *bra:GFP* fluorescence in an *aim*/*aim;chm*/*chm* embryo. Wildtype sibs (not shown) are at late tailbud stage.

(E) Neurula stage wildtype embryo, with phallacidin staining in white and the notochord primordium pseudocolored in red.

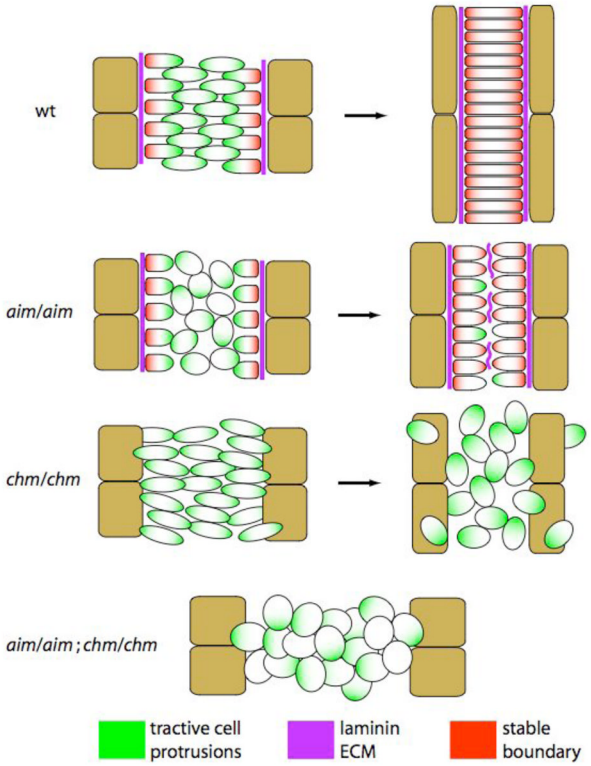

Fig. 6. A model of ascidian notochord morphogenesis

In wildtype embryos, the planar cell polarity pathway mediates mediolateral intercalation behavior and a perinotochordal laminin-containing ECM mediates boundary formation. When the PCP pathway is disrupted in *aim*/*aim* embryos, mediolaterally-biased notochord cell intercalation is perturbed but considerable convergence and extension still slowly occur. This may be the result of randomly moving notochord cells being “trapped” where they stochastically contact the notochord boundary. The PCP pathway is also required to maintain perinotochordal/intranotochordal *Cs*-lamα3/4/5 polarity. The failure of *aim*/*aim* notochord cells to complete the final stages of intercalation may reflect this deposition of laminin on intranotochordal surfaces.

In *chm*/*chm* embryos there is a defect in perinotochordal boundary formation and notochord cells become dispersed in the tail. Despite this morphogenetic defect, there is still a moderate degree of convergence and extension, which is likely due to the PCP pathway given that the *aim*/*aim;chm*/*chm* double mutant shows a near complete failure in convergence and extension. Although the lack of epistasis suggests that the two processes act at least partly in parallel, the true relationship is clearly complex given the role of *aim* in maintaining *Cs*-lamα3/4/5 polarity and the role of *Cs*-lamα3/4/5 in maintaining polarized cell behaviors.